MNRAS **000**, 1–12 (2015) Preprint 13 January 2022 Compiled using MNRAS LATEX style file v3.0

A SCUBA-2 850μm Survey of Heavily Reddened Quasars at $z \sim 2$

Clare F. Wethers[1,2,★], Manda Banerji[2,3], Paul C. Hewett[2], Gareth C. Jones[4,3]
[1] *Finnish Centre for Astronomy with ESO (FINCA), Vesilinnantie 5, FI-20014 University of Turku, Finland*
[2] *Institute of Astronomy, University of Cambridge, Madingley Road, Cambridge, CB30HA, UK*
[3] *Kavli Institute for Cosmology, University of Cambridge, Madingley Road, Cambridge, CB3 0HA, UK*
[4] *Battcock Centre for Experimental Astrophysics, Cavendish Laboratory, Cambridge CB3 0HE, UK*

arXiv:2001.05507v1 [astro-ph.GA] 15 Jan 2020

Accepted XXX. Received YYY; in original form ZZZ

ABSTRACT

We present new 850μm SCUBA-2 observations for a sample of 19 heavily reddened Type-I quasars at redshifts $z \sim 2$ with dust extinctions of $A_V \simeq 2-6$ mag. Three of the 19 quasars are detected at $>3\sigma$ significance corresponding to an 850μm flux-limit of $\gtrsim$4.8 mJy. Assuming the 850μm flux is dominated by dust heating due to star formation, very high star formation rates (SFR) of ~2500-4500 $M_\odot$ yr^{-1} in the quasar host galaxies are inferred. Even when considering a large contribution to the 850μm flux from dust heated by the quasar itself, significant SFRs of ~600-1500 $M_\odot$ yr^{-1} are nevertheless inferred for two of the three detected quasars. We stack the remaining 16 heavily reddened quasars and derive an average 3σ upper limit on the SFRs in these quasar host galaxies of <880 $M_\odot$ yr^{-1}. The number counts of sub-mm galaxies in the total survey area (134.3 arcmin^2) are consistent with predictions from blank-field surveys. There are, however, individual quasars where we find evidence for an excess of associated sub-mm galaxies. For two quasars, higher spatial resolution and spectroscopic ALMA observations confirm the presence of an excess of sub-mm sources. We compare the 850μm detection rate of our quasars to both unobscured, ultraviolet luminous quasars as well as the much more obscured population of mid-infrared luminous Hot Dust Obscured Galaxies (HotDOGs). When matched by luminosity and redshift, we find no significant differences in the 850μm flux densities of these various quasar populations given the current small sample sizes.

Key words: quasars: general – galaxies: evolution – galaxies: star formation – galaxies: high redshift – galaxies: active – submillimetre: galaxies

1 INTRODUCTION

Understanding the interactions between quasars and their host galaxies is critical for constraining models of galaxy evolution. In the local universe, tight correlations have been observed between the mass of the central super-massive black hole (SMBH) and that of the stellar bulge in galaxies (Magorrian et al. 1998; Kormendy & Ho 2013; Gültekin et al. 2009), leading to the idea that black holes and galaxies co-evolve. Both star formation and black-hole accretion also peak at z ~ 2 (e.g. Madau & Dickinson 2014; Aird et al. 2015), further suggesting a link between these two quantities. Whilst the co-evolution of galaxies and quasars is now widely accepted, the exact processes that shape this joint evolution remains an active area of research. Tidal interactions caused by major mergers can drive gas into the central regions of the galaxy, triggering star formation (Sanders et al. 1988; Barnes & Hernquist 1992; Veilleux et al. 2002; Hopkins et al. 2006). As a result of the increased gas supply, the active galactic nucleus (AGN) is able to accrete close to the Eddington limit, appearing highly luminous yet dust-obscured as material from the remnant starburst is blown out from the galaxy. This so-called *blowout* phase (Di Matteo et al. 2005) is postulated to mark the transition between starburst galaxies and ultraviolet-luminous quasars and thus may represent a key phase in the lifetime of a quasar. Studying the connection between dust obscuration, black-hole accretion and star formation in quasars undergoing this transition therefore remains an important test of galaxy evolution models.

In Wethers et al. (2018), we explored the link between star formation as traced by rest-frame ultraviolet (UV) emis-

★ E-mail: clweth@utu.fi

© 2015 The Authors

sion and quasar luminosity in a sample of luminous, yet dust-obscured quasars from (Banerji et al. 2012, 2015a) thought to be seen during the *blowout* phase. These so-called heavily reddened quasars have dust extinctions of $A_V \simeq 2-6$ mags, comparable to what is seen in the sub-millimetre galaxy (SMG) population (Takata et al. 2006). Independent observations of the narrow-line region in these quasars (Temple et al. 2019) as well as ALMA follow-up (Banerji et al. 2017, 2018) suggests that the obscuring dust is likely distributed on galaxy wide scales. In our previous study, we found that these reddened quasars reside in prodigiously star-forming hosts ($SFR_{UV} \sim 100\ M_\odot yr^{-1}$), with the most luminous quasars residing in the most actively star-forming host galaxies. However, the rest-frame UV wavelengths considered in Wethers et al. (2018) trace only the unobscured component of the star formation in the host – potentially accounting for only a small fraction of the total. Long-wavelength observations in the far infrared and at sub-millimetre (sub-mm) wavelengths, tracing cool dust emission, offer the opportunity to study the obscured components of star formation in these systems (e.g. Banerji et al. 2014, 2017). Early studies of UV-luminous high-redshift quasars at sub-mm wavelengths with SCUBA found no strong correlation between the sub-mm and optical luminosity of the quasar at $z \sim 2$ (Priddey et al. 2003) or $z > 4$ (Isaak et al. 2002). More recently, studies of the far infrared-derived star-formation rates in larger samples of AGN covering a wider range in AGN luminosities and using a combination of data from *Herschel* and SCUBA-2 have been undertaken. The results variously reveal either no trend in star-formation rate with quasar luminosity (e.g. Harrison et al. 2012) or, potentially, a correlation between quasar luminosity and star formation rate at the highest luminosities, particularly for populations of obscured quasars (e.g. Rosario et al. 2013; Chen et al. 2013; Banerji et al. 2015b; Stanley et al. 2017). Thus, the link between star formation, quasar luminosity and dust obscuration in high-luminosity, high-redshift quasars still remains unclear.

In this paper we seek to directly test whether the dust obscuration towards the quasar continuum seen in our previously studied population of $z \sim 2$ heavily reddened quasars (Banerji et al. 2012, 2015a; Wethers et al. 2018) is directly linked to the level of obscured star formation in the quasar host galaxy. To this end we have conducted a flux-limited 850μm survey with SCUBA-2 of our heavily reddened quasar population. The paper is structured as follows. Section 2 outlines the sample of heavily reddened quasars and provides detail of the SCUBA-2 850μm observations. Section 3 presents the main results of our study including inferences on obscured star formation in the quasar host galaxies from the 850μm photometry and a study of the environments of our heavily reddened quasars using the SCUBA-2 maps. Section 4 discusses our results in the context of independent studies of similar objects, with our key findings summarised in Section 5. Throughout this work, we adopt a flat ΛCDM cosmology with $H_0 = 70$ km s^{-1} Mpc^{-1}, $\Omega_M = 0.3$ and $\Omega_\Lambda = 0.7$.

2 DATA

The parent population of targets studied in this work is a sample of heavily reddened ($A_V \simeq 2$ - 6 mags), high-luminosity ($L_{bol} \sim 10^{47}$ erg/s) quasars at redshifts of $0.7 < z < 2.7$. The photometric selection and spectroscopic confirmation of these quasars has been presented in Banerji et al. (2012, 2013, 2015a) and Temple et al. (2019) but is summarised briefly below.

2.1 Heavily Reddened Quasars

Heavily reddened quasar candidates were identified in wide-field near-infrared imaging surveys such as the UKIDSS Large Area Survey (ULAS; Lawrence et al. 2007), VISTA Hemisphere Survey (VHS; McMahon et al. 2013) and VIKING (Edge et al. 2013). Targets were required to appear as point-sources in the K-band, with $K_{Vega} < 18.4$[1] to exclude galaxies and isolate the sample of high redshift, near-infrared-luminous quasars. A colour cut of $(J\text{-}K)_{Vega} > 2.5$ was applied to select targets with extremely red near-infrared colours, indicating significant dust reddening ($A_V \simeq 2$ - 6 mags). Spectroscopic confirmation made use of the VLT-SINFONI and Gemini-GNIRS spectrographs and has now resulted in a sample of 63 heavily reddened quasars at $0.7 < z < 2.7$. From these 63 quasars we identified a high-redshift sample with $z > 1.4$, which were also observable from Mauna Kea (Dec > -17 deg). The 19 quasars thus identified, most of which are at $z > 2$, were targeted with SCUBA-2. With extinction-corrected bolometric luminosities of $L_{bol} \sim 10^{47}$ergs^{-1} and $M_{BH} \sim 10^{9-10}$ $M_\odot$ (Banerji et al. 2015a), the objects are among the most luminous and massive accreting SMBHs known at z~2.

2.2 SCUBA2 Observations and Data Reduction

SCUBA-2 is a dual wavelength camera, operating at 450μm for the short waveband and 850μm for the long waveband, with diffraction-limited beam full-width half maxima (FWHM) of approximately 9.8- and 14.6 arcsec respectively. Each of the two focal planes comprise four sub-arrays of 1280 bolometers, totalling 5120 pixels in each plane (Holland et al. 2013).

The 19 quasar targets were observed with SCUBA-2 on the 15m *James Clerk Maxwell Telescope* (JCMT) on Mauna Kea, Hawaii, between 2017 March and May. Each target was observed in the 'CV Daisy' observing mode, which is suitable for point-like sources or sources with structure on scales < 3 arcmin. The CV Daisy observing-mode produces a 12 arcmin diameter map, with the deepest coverage in the central 3 arcmin diameter region, where all four sub-arrays overlap (Holland et al. 2013). Details of the 19 reddened quasars observed with SCUBA-2 are given in Table 1. The exposure time for each observation ranges between 25 and 37 minutes, reaching a 1σ noise level of $\sim 1.1-2.6$ mJy.

The 850μm SCUBA-2 observations are reduced with the STARLINK SubMillimetre User Reduction Facility (SMURF)

[1] Magnitudes were calculated within a 1 arcsecond radius aperture (*apermag3*) and include an aperture correction appropriate for point sources.

data reduction package. We used the 'REDUCE_SCAN_FAINT_POINT_SOURCES' recipe, which uses a 'blank field' configuration suitable for point sources with low signal-to-noise ratio (Chapin et al. 2013). Initial pre-processing is carried out by the SMURF software, which cleans the data by modelling the signal contributions from each bolometer, removing unwanted atmospheric emission and re-gridding the data to produce a science-quality image. Each of these science-quality images are then combined as a mosaic, centred on the sky position of the source, by the PIpeline for Combining and Analysing Reduced Data (PICARD). Finally, a beam-matched filter is applied to the resulting mosaicked image, smoothing the image with a 15 arcsec FWHM Gaussian and calibrating the resulting map with a flux conversion factor of 2.34 Jy $pW^{-1}arcsec^{-2}$ (appropriate for point sources). In this way, 850μm maps are created for each of the 19 reddened quasars in our sample. Finally, the astrometry and photometry of the resulting SCUBA-2 maps are checked via the reduction of the pointing and flux calibrators through the same pipeline. The noise level for each map is derived from the median of the error map of each observation (cropped to cover the same region as the 850μm signal maps) using the Kernel APplication PAckage (KAPPA) within the STARLINK software.

3 RESULTS

3.1 850μm Photometry

From the reduced SCUBA-2 850μm maps, we calculate peak flux densities for the 19 quasar targets using a 14.6 arcsec diameter aperture, centred on the quasar, which matches the beam size of SCUBA-2. These values are given in Table 1 along with the corresponding 1σ noise on each measurement. Of the 19 quasars, only three sources are detected at >3σ confidence. These are ULASJ1216-0313, ULASJ2200+0056 and ULASJ2315+0143 and the corresponding 850μm maps can be seen in Fig. 1. We note that the peak sub-mm flux for ULASJ2200+0056 appears to be spatially offset from the quasar centroid. Nevertheless we class this source as a detection as the peak sub-mm flux lies within one SCUBA-2 beam from the quasar position.

Fourteen of the remaining 16 quasar targets, which lie below the 3σ detection limit nevertheless have a positive 850μm peak flux density within a beam-sized aperture centred on the near-infrared position of the quasar, with a significance of ~1.1σ. To explore the average sub-mm properties of our sample we stack all 16 undetected sources, which all lie at z~2. An inverse variance weighting is applied to the stack to account for noise variations between objects i.e.

$$S_{\rm ij} = \frac{\sum_{\rm k=1}^{\rm N} P_{\rm ij}^{\rm k} \times f_{\rm ij}^{\rm k}/(\sigma_{\rm ij}^{\rm k} \times \sigma_{\rm ij}^{\rm k})}{\sum_{\rm k=1}^{\rm N} P_{\rm i,j}^{\rm k}/(\sigma_{\rm ij}^{\rm k} \times \sigma_{\rm ij}^{\rm k})}, \quad (1)$$

where i, j denote the pixel coordinates with respect to the catalogued quasar position. P_{ij} is the response function of SCUBA-2 at 850μm, taken to be the PSF for each observation produced by the STARLINK reduction software, f_{ij} are the flux densities for each of the N sources in our sample and σ_{ij} are the corresponding noise maps, provided independently from the combined signal + noise maps during the reduction (Sec. 2.2). The resulting stacked image is shown in Fig. 2, from which we derive a peak flux density of 0.85 ± 0.41 mJy. The uncertainty on the stacked flux has been derived by looking at the standard deviation of the pixels over a blank portion of the stacked image prior to the PSF weighting. The stacked image therefore does not show a significant detection. However the average 850μm flux density derived for this small sample is consistent with Banerji et al. (2015b), who have studied the average 850μm properties of a much larger sample of 699 X-ray luminous AGN and find a significant stacked flux density of 0.71±0.08 mJy.

3.2 Dust-Obscured Star Formation

Based on the photometry in Table 1, we now derive star formation rates for the three sources in our sample detected at 850μm - ULASJ1216-0313, ULASJ2200+0056 and ULASJ2315+0143 - as well as an upper limit on the star formation rate based on the stacked non-detections (Fig. 2). We assume for now that the cold dust component traced by the 850μm flux density at these redshifts is being heated entirely by star formation although see Symeonidis (2017) and Section 3.2.1 for an alternative explanation. The far-infrared to sub-mm spectral energy distributions (SEDs) of our quasars can then be modelled using a single grey-body template, characterised by three parameters; the dust temperature, T, the emissivity index, β and the overall normalisation, $f_{\rm GB}$, such that

$$S_\nu({\rm mJy}) = {\rm f_{GB}} \times (1 - {\rm e}^{\tau(\nu)}) \times \frac{\nu^3}{{\rm e}^{\frac{{\rm h}\nu}{{\rm kT}}} - 1}, \quad (2)$$

where the optical depth, $\tau(\nu)$, is given as a function of ν_0 - the frequency at which $\tau(\nu) = 1$, i.e.

$$\tau(\nu) = \left(\frac{-\nu}{\nu_0}\right)^\beta. \quad (3)$$

In high-redshift star-forming galaxies the dust temperatures lie in the range $20 \lesssim T \lesssim 60$ K (e.g. Casey 2012), whereas in quasar host galaxies the dust is usually hotter, T~40-50K (Priddey & McMahon 2001; Beelen et al. 2006). Given the single photometric data point at 850μm available for our quasars we use two fixed combinations of T and β appropriate for high-redshift quasars: (i) T=47K, β=1.6 (Priddey & McMahon 2001) and (ii) T=41K, β=1.95 (Beelen et al. 2006). Each greybody model is then fit in turn to the photometry of ULASJ1216-0313, ULASJ2200+0056 and ULASJ2315+0143, with the overall normalisation left as a free parameter in the fitting. The resulting grey-body fits are shown in Fig. 3. The shaded regions in each of the greybody templates denote the 1σ uncertainty in each fit, derived from fitting the upper and lower 1σ bounds of the photometry.

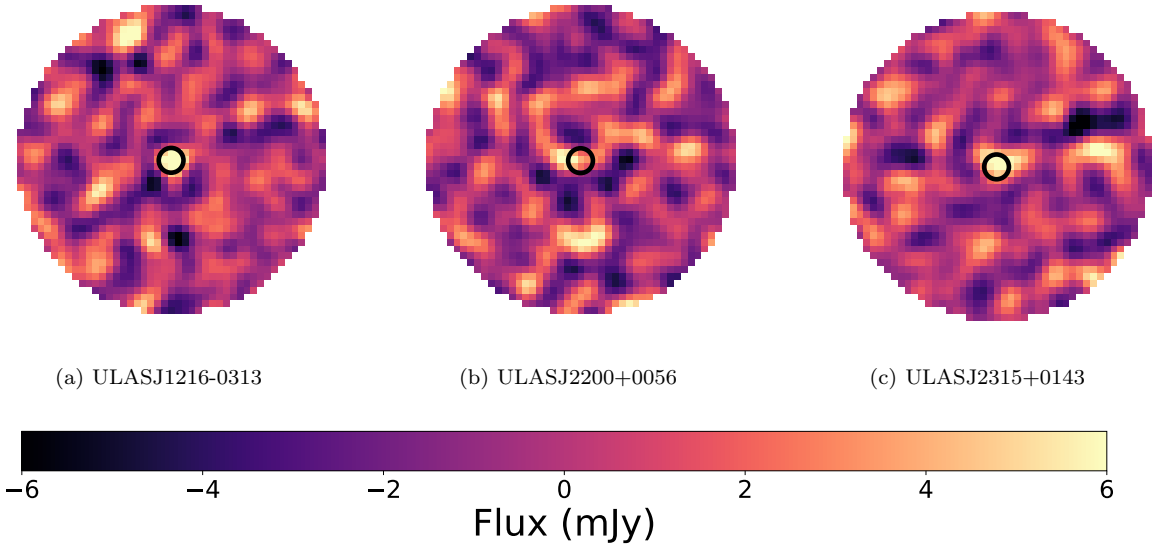
From the resulting grey-body templates, we derive estimates for the far infrared luminosity:

$$L_{\rm FIR} = 4\pi D_{\rm L}^2 \int_{\nu_{\rm min}}^{\nu_{\rm max}} S(\nu) d\nu, \quad (4)$$

where D_L is the luminosity distance, ν_{min} and ν_{max} denote the frequency limits of the integral (ν_{min} = 1.0 THz; ν_{max} = 7.5 THz, corresponding to wavelengths 40μm < λ < 300μm)

Table 1. SCUBA-2 observation log for the 19 heavily-obscured quasars, including the 850μm flux densities and associated uncertainties derived in Section 3.1.

Name	RA	DEC	Observation Date	Exposure Time (HH:MM:SS)	$S_{850} \pm \sigma_{850}$ (mJy)	$\log_{10}[L_{bol}]$ ($ergs^{-1}$)	Redshift
ULASJ0016-0038	4.0025	-0.6498	2017.05.06	00:32:28	0.15 ±1.73	46.9	2.194
ULASJ0041-0021	10.3041	-0.3520	2017.05.06	00:32:32	0.74 ±1.70	47.3	2.517
VHSJ1117-1528	169.2656	-15.4749	2017.04.17	00:36:47	0.52 ±2.64	47.6	2.427
VHSJ1122-1919	170.6018	-19.3215	2017.04.17	00:36:47	-0.04 ±1.62	47.6	2.465
ULASJ1216-0313	184.1324	-3.2264	2017.04.16	00:32:14	9.90 ±1.82	48.3	2.576
ULASJ1234+0907	188.6147	9.1317	2017.04.16	00:30:40	2.46 ±2.03	48.5	2.503
VHSJ1301-1624	195.3805	-16.4150	2017.04.17	00:36:53	2.49 ±1.62	47.4	2.140
VHSJ1350-0503	207.6552	-5.0665	2017.04.18	00:33:45	0.71 ±1.85	47.2	2.176
VHSJ1409-0830	212.3721	-8.5163	2017.04.18	00:34:49	3.26 ±1.70	47.1	2.300
ULASJ1455+1230	223.8375	12.5024	2017.05.04	00:31:10	2.53 ±1.85	47.2	1.460
ULASJ1539+0057	234.7923	5.9638	2017.04.04	00:30:57	4.06 ±1.53	48.2	2.658
VHSJ1556-0835	239.1571	-8.5952	2017.04.17	00:33:55	1.69 ±1.58	47.0	2.188
VHSJ2109-0026	317.3630	-0.4497	2017.04.03	00:32:02	1.51 ±1.59	46.9	2.344
VHSJ2143-0643	325.8926	-6.7206	2017.03.30	00:33:57	0.68 ±1.54	47.1	2.383
VHSJ2144-0523	326.2394	-5.3881	2017.04.04	00:25:09	0.75 ±1.10	46.7	2.152
ULASJ2200+0056	330.1036	0.9346	2017.04.17	00:32:27	5.92 ±1.64	47.4	2.541
ULASJ2224-0015	336.0392	-0.2566	2017.04.18	00:32:04	-1.83 ±2.00	47.0	2.223
ULASJ2315+0143	348.9843	1.7307	2017.05.05	00:32:32	6.43 ±1.58	47.5	2.560
VHSJ2355-0011	358.9394	-0.1893	2017.05.06	00:32:25	3.66 ±1.72	47.2	2.531



(a) ULASJ1216-0313 (b) ULASJ2200+0056 (c) ULASJ2315+0143

Figure 1. 850μm SCUBA-2 maps for the three sources detected at a significance >3σ - ULASJ1216-0313, ULASJ2200+0056 and ULASJ2315+0143. Black circle denotes a 14.6-arcsec diameter aperture centred on the SCUBA-2 position of the target source. North is up, East is to the left.

and $S(\nu)$ is the best-fit grey-body. We use L_{FIR} - tracing the emission at 40μm < λ < 300μm - rather than the total infrared luminosity in order to minimise contamination from dust heating by the quasar, which can significantly contribute to the flux at λ < 40μm. The key assumption is that the cooler dust, peaking at wavelengths >40μm, is predominantly heated by star formation. The SFR for each system is then derived using the relation from Kennicutt Jr & Evans (2012):

$$SFR = 3.89 \times 10^{-44} \times L_{\rm FIR}, \quad (5)$$

where the SFR is given in units of $M_{\odot}yr^{-1}$ and L_{FIR} is in units of erg/s.

The SFRs based on the two different greybody assumptions for the three detected quasars and the 3σ upper limits from the stacked non-detection are given in Table 2. In the case of the three 850μm detections, these SFRs are

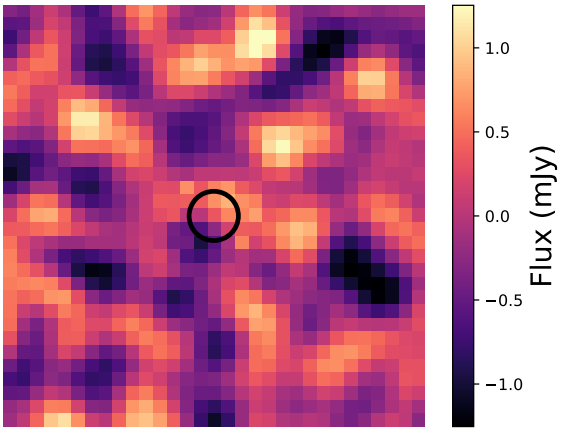
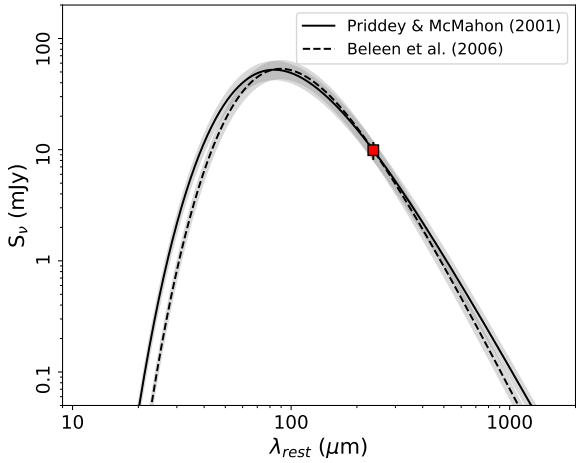


Figure 2. Inverse variance weighted stack for the 16 undetected targets in our sample. Peak flux of 0.85 ± 0.41 mJy (~2.0σ) within a 14.6 arcsec SCUBA-2 beamsize.

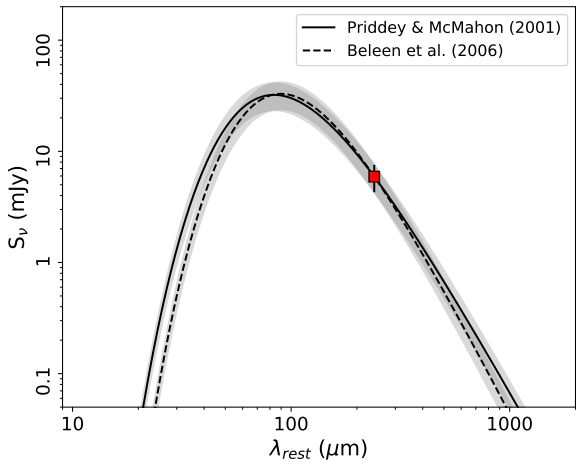
Table 2. SFRs for the targets detected at >3σ confidence at 850μm, based on greybody template fitting with parameters from Priddey & McMahon (2001) (SFR_P) and Beelen et al. (2006) (SFR_B). For the 16 remaining non-detections, we derive 3σ upper limits on the SFR based on each template.

Name	SFR_P ($M_\odot yr^{-1}$)	SFR_B ($M_\odot yr^{-1}$)
ULASJ1216-0313	4450 ± 820	4080 ± 750
ULASJ2200+0056	2650 ± 730	2430 ± 670
ULASJ2315+0143	2880 ± 710	2650 ± 650
Stacked non-detections	< 880	< 830

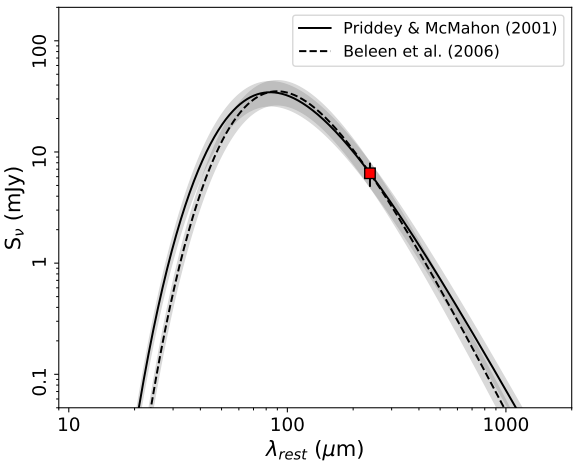
found to be very large - ~2500-4500 $M_\odot$ yr^{-1}. Such high SFRs are not uncommon in the most luminous quasars detected at sub-mm wavelengths (e.g. Isaak et al. 2002; Priddey et al. 2003; Stacey et al. 2018) and even higher SFRs have been claimed in populations of hyperluminous infrared galaxies (HyLIRGs; Rowan-Robinson et al. 2018). However, the three quasars detected at 850μm are also among the most luminous quasars in our sample and it is possible that the quasar itself could be contributing to the dust heating at 850μm, which would reduce the inferred SFRs. Later, in Section 3.2.1, we discuss the potential effects of this quasar contamination on our results. Two of the three quasars, ULASJ2200+0056 and ULASJ2315+0143 also showed evidence for residing in star-forming host galaxies based on our rest-frame ultraviolet detections of the quasar hosts in the Dark Energy Survey (Wethers et al. 2018). The ultraviolet-derived star formation rates for these two quasars are among the highest in our sample - SFR_{UV} ~ 200 − 400$M_\odot$ yr^{-1}. Nevertheless, the sub-mm derived star formation rates are significantly higher, implying that a large fraction of the star formation in heavily reddened quasar hosts is obscured by dust. From the stacked non-detection of our remaining 850μm undetected quasars, we derive a 3σ upper limit on the SFR of $\lesssim$850 $M_\odot$ yr^{-1}. We therefore note that while the majority of our heavily reddened quasars are undetected with SCUBA-2, this does not preclude significant levels of star formation in these systems.



(a) ULASJ1216-0313



(b) ULASJ2200+0056



(c) ULASJ2315+0143

Figure 3. Grey-body fit to the 850μm photometry of ULASJ1216-0313 (a), ULASJ2200+0056 (b) and ULASJ2315+0143 (c) assuming (i) T=47K, β=1.6 (Priddey & McMahon 2001) *(solid)* and (ii) T=41K, β=1.95 (Beelen et al. 2006) *(dashed)*. Shaded regions represent the 1σ uncertainty on each fit.

3.2.1 Quasar Heating

In Section 3.2, we derive SFRs for the three quasars detected with SCUBA2, assuming the cold dust at 850μm is entirely heated by star formation. However, several studies suggest that a significant fraction of the emission at this wavelength may still be attributed to heating from the quasar, particularly in very luminous systems (e.g. Mor & Netzer 2012; Symeonidis et al. 2016; Mullaney et al. 2012; Lyu et al. 2017; Lyu & Rieke 2017). To illustrate the level of uncertainty arising from the potential quasar contamination at 850μm, we make use of the quasar template provided in Mor & Netzer (2012), based on the intrinsic SEDs of 115 nearby Type-1 AGN with luminosities $L_{5100} \simeq 10^{43.2}$-$10^{45.9}$ ergs^{-1}. The model is scaled to photometry from the Wide-field Infrared Survey Explorer (WISE) in four wavebands (W1;λ3.4μm, W2;λ4.6μm, W3;λ12μm and W4;λ22μm) and normalised at 6μm (Fig. 4). Based on this scaling, the contribution of the quasar to the 850μm flux of the three detected quasars (ULASJ1216-0313, ULASJ2200+0056 and ULASJ2315+0143) is estimated and subtracted from the original SCUBA2 photometry, and this new photometry is modelled with a modified blackbody curve following the methods outlined in Sec. 3.2. Based on the model of Mor & Netzer (2012), we find minimal quasar contamination at 850μm for all three of the quasars detected with SCUBA2, deriving quasar-subtracted SFRs within ~5 per cent of the original estimates in Tab. 2 - SFR = 4320±710 (3970±750) $M_\odot yr^{-1}$, 2560±730 (2360±670) $M_\odot yr^{-1}$ and 2720±710 (2500±650) $M_\odot yr^{-1}$ for ULASJ1216-0313, ULASJ2200+0056 and ULASJ2315+0143 respectively, based on the parameters in Priddey et al. (2003) (and Beelen et al. 2006)

Other studies however estimate much higher levels of quasar contamination at 850μm. Symeonidis et al. (2016), for example, find that the contribution of quasar heating may be comparable to that of star formation out to $\lambda <$ 1000μm. As we do not have enough sample specific information to constrain the exact level of quasar contamination in our sample, we additionally make use of the quasar SED in Symeonidis et al. (2016), which includes the largest quasar contribution to the cool dust emission of quasar templates available in the literature and therefore provides the most conservative estimate of the SFR. Again, the quasar template is scaled to the WISE photometry of the three detected quasars (Fig. 4) and the quasar contribution at 850μm is subtracted from the SCUBA2 flux. Fitting a greybody curve to this new photometry returns significantly lower SFRs than derived in Sec. 3.2. When accounting for the quasar contamination estimated by the Symeonidis et al. (2016) model, we derive SFR = 1570±820 (1440±750) and 690±730 (630±670) $M_\odot yr^{-1}$ for ULASJ1216-0313 and ULASJ2200+0056 respectively, based on the parameters in Priddey et al. (2003) (and Beelen et al. 2006), whilst all the 850μm flux observed in ULASJ2315+0143 can be accounted for by the Symeonidis et al. (2016) model.

Despite deriving SFRs a factor of >2.5 lower than those in Section 3.2, in which all cool dust is attributed to star formation, both ULASJ1216-0313 and ULASJ2200+0056 continue to show evidence for prolific star formation. Based on the model in Symeonidis et al. (2016) however, we cannot rule out that the 850μm flux of ULASJ2315+0143 derives entirely from quasar heating. However, ALMA observations of ULASJ2315+0143 (Banerji et al. 2018) have detected the dust continuum emission from this source at an observed frame wavelength of 1.2mm (rest-frame ~330 μm) where contributions from quasar heating are expected to be negligible even when considering the most extreme quasar models. Full SED modelling of this source in Banerji et al. (2018) leads to an estimated star formation rate of 680 $M_\odot yr^{-1}$. The source is additionally shown to be a close separation merger of two separate dusty galaxies. Thus at least some of the 850um emission in ULASJ2315+0143 is likely to be originating from dust heated by star formation. Whilst the effects of quasar contamination may significantly alter the SFRs derived for our quasar sample, we therefore maintain that the dusty quasars detected with SCUBA2 show evidence for prolific star formation.

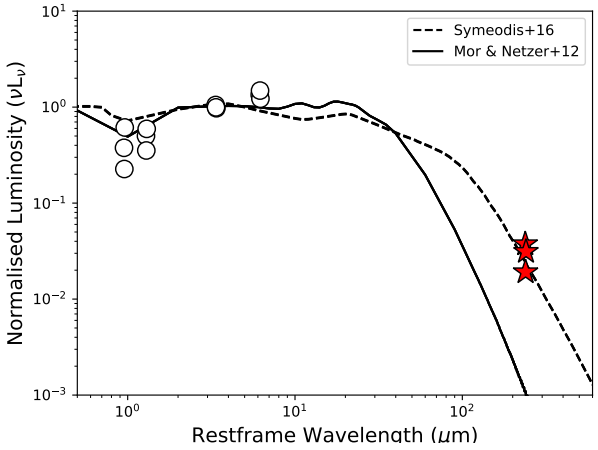


Figure 4. Quasar SEDs from Mor & Netzer (2012) *(solid line)* and Symeonidis et al. (2016) *(dotted line)*, fitted to the WISE photometry of our detected quasar sample *(white dots)* and normalised at 6μm. The SCUBA2 photometry *(red stars)* is overlaid for reference.

3.3 Reddened Quasar Environments

Whilst the majority of our reddened quasar sample are undetected at 850μm, inspection of the maps reveals a number of serendipitous sub-mm detections within a 1.5 arcmin radius of the quasar targets, potentially indicating an environmental overdensity on scales < 1Mpc. To investigate this and to identify any serendipitous detections, we look for >3σ peaks in the signal-to-noise ratio maps. Any sources lying at the edge of the maps were omitted from the source counts.

Table 3 shows the number of serendipitous detections found above 3, 3.5 and 4σ across our full sample, along with the corresponding number of negative detections for the same detection threshold. Although some negative sources are expected due to 'bowling' around real positive sources in the SCUBA-2 images, we find the number of these negative sources to make up half of the positive sources detected at >3σ, meaning that only half of these positive sources are likely to be real. At 3.5σ, the number of negative sources drops to 38 per cent of the positive detections, with no maps containing multiple negative detections. When the detection threshold is further increased to 4σ, the negative sources ac-

count for just 25 per cent of the positive detections, meaning the majority of sources detected above this threshold are unlikely to be artefacts of the noise in the image. Fig 5 shows the location of all 3.5 and 4σ 850μm detections in all 19 of our SCUBA-2 maps.

In total, we find 24 (12) sub-mm sources at >3.5σ (>4σ) across our reddened quasar sample, corresponding to a total survey area of 134.3 arcmin^2. To test whether this is indicative of an overdensity, the number counts for the >3.5σ ($\gtrsim$5.6 mJy) and >4σ ($\gtrsim$6.4 mJy) detections are directly compared to sub-mm blank field samples (Geach et al. 2017) by plotting the cumulative frequency of the source counts as a function of their 850μm flux (Fig. 6). Using the number counts of the positive and negative sources in Table 3, we expect 62 per cent of the 3.5σ and 75 per cent of the 4σ detections to be real. We account for this when comparing to the sub-mm blank fields in Fig. 6 by scaling the number of sources by the fraction we predict to be real.

Fig. 6 shows that at both >3.5 and >4σ the source counts in our reddened quasar survey are entirely consistent with those in the blank fields when averaging over the full survey area for our sample of 19 reddened quasars. However, there are clearly individual fields where we do see some evidence for over-densities. For example, above our 3.5σ flux-limit of $\simeq$5.6 mJy we would predict 0.5 sources within a single SCUBA-2 map of radius 1.5 arcmin based on the Geach et al. (2017) blank-field counts. There are four quasars where we see two or three sources in the SCUBA-2 maps brighter than this flux-limit (Table 3). Even accounting for the false detection rate of 38 per cent at this threshold, there are still 1-2 real sources detected around the quasar in these fields, a factor of 2-4 higher than predicted from the blank-field counts. It is thus reasonable to conclude that while the majority of our reddened quasars do not appear to reside in over-dense regions, there are nevertheless examples of heavily reddened quasars that may do. It should also be noted that any sub-mm sources $\lesssim$30 arcsec away from the quasar will not be resolved as a separate source in the SCUBA-2 images and may be blended with the quasar emission. As discussed in the following sub-section, higher spatial resolution Atacama Large Millimetre Array (ALMA) observations for two quasars confirm the presence of close companions.

3.3.1 Multiplicity from ALMA

Two of the reddened quasars in our sample (ULASJ1234+0907 and ULASJ2315+0143) have also been observed with ALMA (Banerji et al. 2017, 2018) in Band 3 and Band 6, which trace the 1.24mm and 2.92mm continuum emission. With the higher resolution of the ALMA observations ($\simeq$2-3 arcsec compared to $\simeq$15 arcsec with SCUBA-2), Banerji et al. (2018) find that both ULASJ1234+0907 and ULASJ2315+0143 have multiple sources present near the quasar. The locations of the ALMA continuum detected sources are overlaid on the SCUBA-2 850μm maps in Fig. 7. With ALMA, Banerji et al. (2018) also detect multiple molecular emission lines from these sources and in both ULASJ1234+0907 and ULASJ2315+0143. The additional ALMA sources marked in Fig. 7 are found to lie at a similar redshift to the quasar, confirming that they are part of the same overdensity. This provides direct evidence that at least some fraction of the reddened quasars in our sample reside in high density sub-mm environments. We note that ULASJ1234+0907 is undetected with SCUBA-2, lying below the 3σ detection limit of our sample. However, the two companion galaxies near the quasar appear to have higher 850μm flux densities (7.48±2.03 mJy and 5.92±2.03 mJy) than the quasar.

Fig. 7 shows that both the ALMA sources detected in the map of ULASJ2315+0143 lie within the beamsize of SCUBA-2, so the SCUBA-2 850μm flux density represents the sum of the two ALMA sources. The same may also be true for the other two heavily reddened quasars detected at 850μm. Indeed, in the case of ULASJ2200+0056, the 850μm peak is offset from the quasar position, which could indicate that the bulk of the sub-mm emission is not associated with the quasar but rather a companion galaxy.

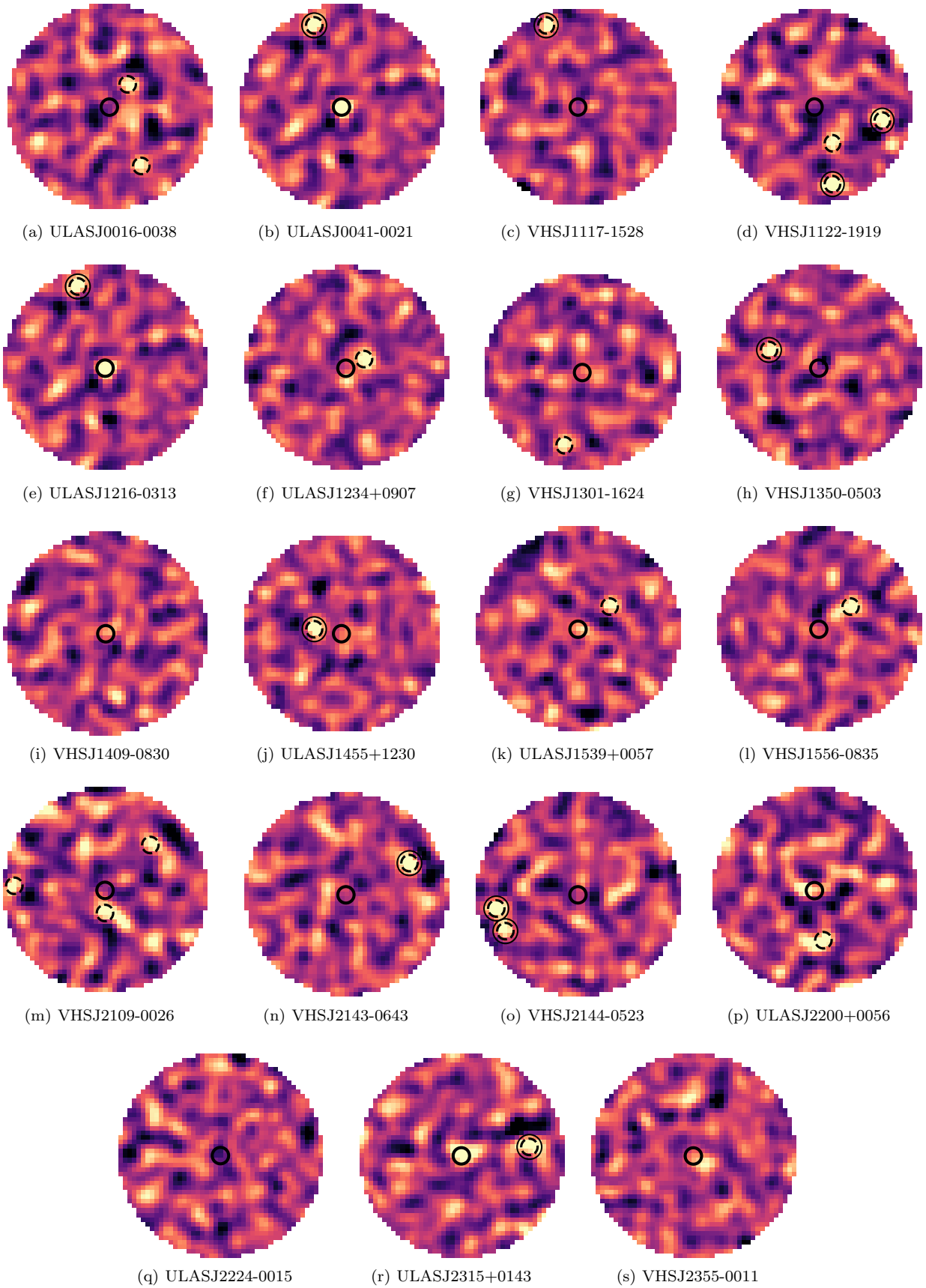
4 DISCUSSION

In order to put our new 850μm observations of the heavily reddened quasar population at $z \sim 2$ in context, we compare the results to similar observations of other high-redshift, high-luminosity quasars. In particular, we consider a sample of UV-luminous, essentially unobscured, quasars observed with SCUBA (Priddey et al. 2003) as well as the population of mid-infrared luminous Hot Dust Obscured Galaxies (Hot-DOGS; Eisenhardt et al. 2012) discovered using the *WISE* All-Sky Survey, which have considerably higher line of sight extinctions compared to our reddened quasars.

4.1 UV-Luminous Unobscured Quasars

Priddey et al. (2003) conducted a large 850μm survey of 57 UV-luminous quasars at $z \sim 2$ with SCUBA down to a relatively bright 3σ flux-limit of 10 mJy. Only nine of the 57 quasars were detected at 850μm in their study. In Fig. 8 we compare the quasar bolometric luminosity and redshift distribution of our sample with the UV-bright quasars from Priddey et al. (2003). In the case of our sample, L_{bol} is derived from the dust-corrected flux at 5100Å after applying a bolometric correction factor of 7 (Vestergaard & Peterson 2006). While the redshift range of our quasars overlaps with the UV-bright quasars, overall our dusty quasars are intrinsically fainter than the UV-luminous quasars. Our 850μm survey also probes a factor of two deeper than the SCUBA survey, reaching a 3σ flux-limit of ~4.8 mJy.

Nine of the 57 UV-luminous quasars presented in Priddey et al. (2003) are brighter than 10mJy, corresponding to 16 per cent of their full sample. By comparison, none of our heavily reddened quasars are detected above this flux threshold, although ULASJ1216-0313 has a flux-density of 9.9±1.8 mJy, consistent with a >10mJy flux given the 1σ uncertainties. Overall therefore it appears that a smaller fraction of our quasar sample is extremely sub-mm bright compared to the UV-luminous quasars in Priddey et al. (2003). We note however that the median dust-corrected L_{bol} of our sample is $10^{47.2}$ ergs^{-1}, compared to $10^{47.7}$ ergs^{-1} in the sample of Priddey et al. (2003). The lower sub-mm detection rate for quasars in our sample could therefore potentially be explained by their lower luminosities. If we only consider quasars with $L_{bol} > 10^{47.25}$ ergs^{-1}, which includes the entire Priddey et al. (2003) sample, the 850μm detection rates for



(a) ULASJ0016-0038 (b) ULASJ0041-0021 (c) VHSJ1117-1528 (d) VHSJ1122-1919

(e) ULASJ1216-0313 (f) ULASJ1234+0907 (g) VHSJ1301-1624 (h) VHSJ1350-0503

(i) VHSJ1409-0830 (j) ULASJ1455+1230 (k) ULASJ1539+0057 (l) VHSJ1556-0835

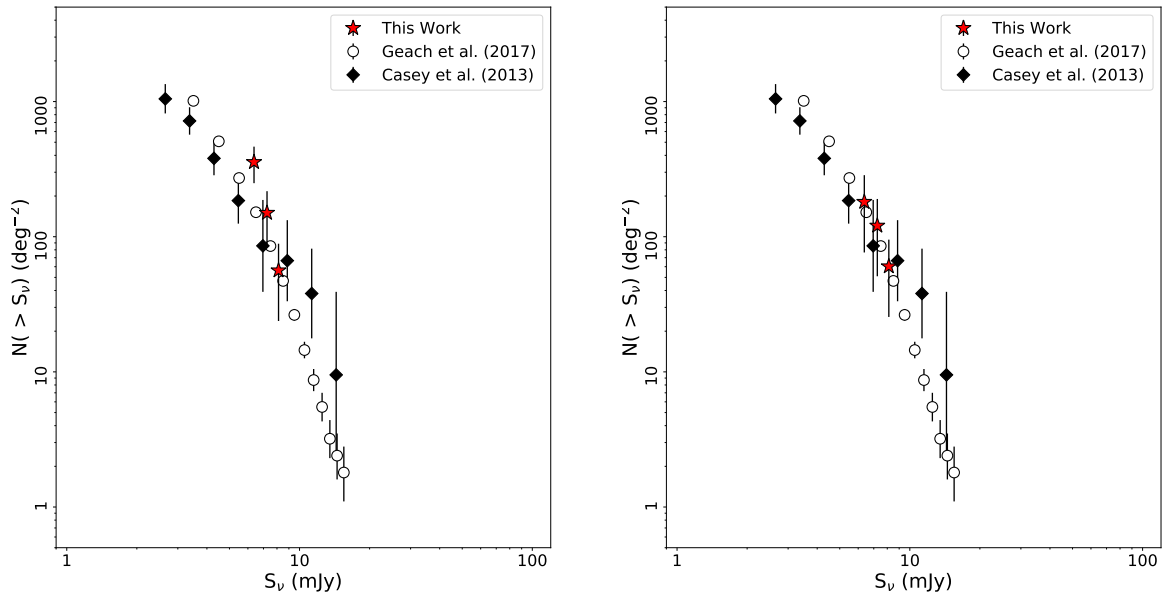
(m) VHSJ2109-0026 (n) VHSJ2143-0643 (o) VHSJ2144-0523 (p) ULASJ2200+0056

(q) ULASJ2224-0015 (r) ULASJ2315+0143 (s) VHSJ2355-0011

Figure 5. Three-arcminute diameter maps for all quasar targets, showing the locations of serendipitous sources detected at >3.5σ (*dotted*) and >4σ (*solid*). Central aperture denotes the 14.6 arcsec diameter SCUBA-2 beam at the position of each quasar in our sample. North is up, East is to the left.

Table 3. Number counts for positive and negative sources lying within a 1.5 arcmin radius of each quasar target, detected with a significance above 3, 3.5 and 4σ.

Name	>3.0σ	<-3.0σ	>3.5σ	<-3.5σ	>4.0σ	<-4.0σ
ULASJ0016-0038	3	2	2	1	0	0
ULASJ0041-0021	4	2	0	1	0	1
VHSJ1117-1528	1	0	1	0	1	0
VHSJ1122-1919	5	2	3	1	2	0
ULASJ1216-0313	3	2	2	1	2	0
ULASJ1234+0907	1	0	1	0	0	0
VHSJ1301-1624	3	0	1	0	0	0
VHSJ1350-0503	1	2	1	0	1	0
VHSJ1409-0830	2	1	0	0	0	0
ULASJ1455+1230	1	1	1	1	1	0
ULASJ1539+0057	1	1	1	0	0	0
VHSJ1556-0835	2	0	1	0	0	0
VHSJ2109-0026	5	2	3	1	0	0
VHSJ2143-0643	1	2	1	1	1	0
VHSJ2144-0523	2	1	2	0	2	0
ULASJ2200+0056	3	1	2	0	0	0
ULASJ2224-0015	0	2	0	0	0	0
ULASJ2315+0143	3	2	2	1	2	1
VHSJ2355-0011	1	1	0	1	0	1
TOTAL	42	24	24	9	12	3



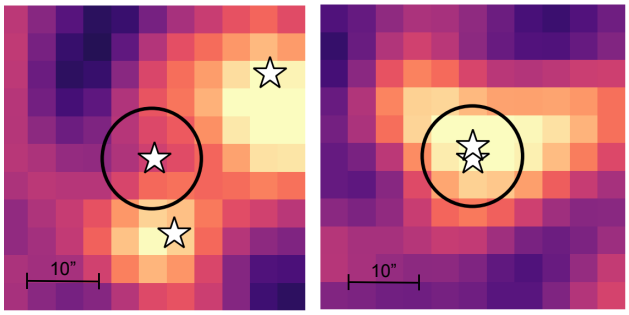
(a) >3.5σ (b) >4.0σ

Figure 6. >3.5σ (a) and >4σ (b) detections within 1.5 arcmin radius of the reddened quasar targets (red stars) are compared to the blank-field counts from Geach et al. (2017) (open circles) and Casey et al. (2013) (solid diamonds). Number counts for our sample have been corrected to represent only the fraction of 'real' sources expected based on the statistics provided in Table 3.

the two samples are consistent given the small number of detections.

4.2 Mid-Infrared Luminous HotDOGs

Jones et al. (2014) outline a sample of ten HotDOGs, selected from the *WISE* All-Sky Survey, with dust extinctions of $A_V \gtrsim 15$ mag towards the quasar continuum – significantly larger than the $A_V \simeq$ 2-6 mag values for our sample. Of the ten HotDOGs (Jones et al. 2014), eight have spectroscopic redshifts within the range of our reddened quasar sample ($1.4 < z < 3$) and therefore form our comparison sample. In order to make a direct comparison to the reddened quasar population, we select only the seven quasars in our sample with 22μm (W4) magnitudes brighter than 8.0 (Vega), above which the entire Jones et al. (2014) sam-



(a) ULASJ1234+0907 (b) ULASJ2315+0143

Figure 7. SCUBA2 maps for the two sources in our sample also observed with ALMA – ULASJ1234+0907 and ULASJ2315+0143. White stars denote the location of individual sources detected with higher-resolution ALMA data (Banerji et al. 2017). North is up, East is to the left.

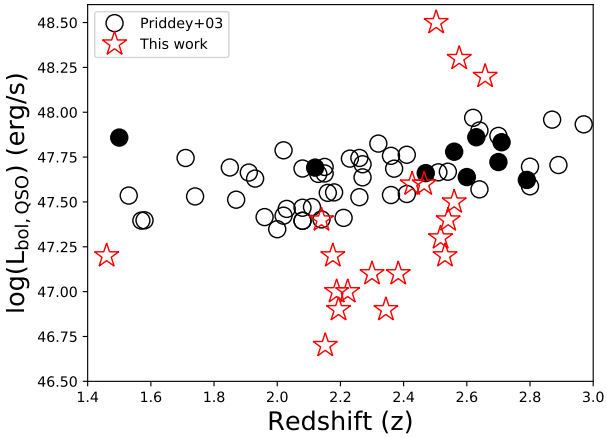


Figure 8. A comparison of the bolometric quasar luminosities (L_{bol}) for our sample (*red stars*) and the UV-luminous quasar sample of Priddey et al. (2003) (*black circles*). Filled symbols denote all sources detected above a flux limit >10mJy, corresponding to the 3σ detection threshold in Priddey et al. (2003). The quasar luminosities in our sample have been corrected for the effects of dust.

ple lies. The redshifts and 22μm (W4) magnitudes for the two samples are presented in Fig. 9.

Two of the eight HotDOGs (25 per cent) are detected at an 850μm flux-limit brighter than 5.8 mJy, corresponding to the 3σ detection threshold used in this paper. By comparison, three of the seven heavily reddened quasars (43 per cent) with W4 magnitudes brighter than 8.0 (Vega) are detected at 850μm above this flux threshold. Furthermore, a second sample of 30 HotDOGs is outlined by Jones et al. (2015), in which targets are additionally required to be detected as compact radio sources. Although only four of these radio-selected HotDOGs have spectroscopic redshifts within the range of our reddened quasar sample, we note that none are detected >5.8 mJy at 850μm. Given the small numbers of detections however, there is no statistically significant evidence for a difference in the 850μm detection rates between HotDOGs and reddened quasars.

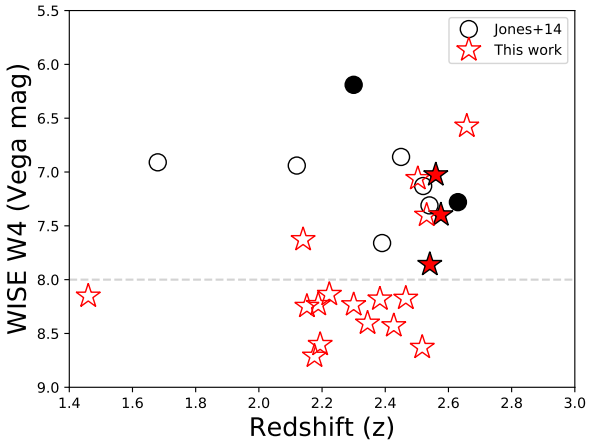


Figure 9. A comparison of the WISE W4 magnitudes (Vega) of our quasar sample (*red stars*) and the HotDOGs from Jones et al. (2014) (*black circles*). Filled symbols denote all sources detected above a flux limit >5.8 mJy, corresponding to the 3σ detection threshold in our sample. The HotDOG W4 magnitude-selection cut at 8 mag is also shown (*grey line*)

In Section 3.3 we concluded that our heavily reddened quasars do not, on average, reside in over-dense regions of the universe although some individual quasars may do. Similar studies have been conducted for the HotDOG populations in Jones et al. (2014, 2015), who find evidence for over-densities around their AGN. The over-densities appear to be more pronounced in the radio-selected HotDOG population. However, many of the radio-HotDOGs from Jones et al. (2015) lack spectroscopic redshifts and thus it is difficult to make a more direct comparison using luminosity- and redshift-matched samples.

5 CONCLUSIONS

We have presented new 850μm SCUBA-2 observations for a sample of 19 luminous, heavily reddened quasars ($A_V \simeq$ 2-6 mags) at $1.4 \leq z \leq 2.7$ – the peak epoch of both star formation and black hole accretion.

(i) Three of the 19 quasars are detected at >3σ significance corresponding to 850μm flux densities of >4.8 mJy. Assuming the 850μm emission is dominated by cool dust heated by star formation in the quasar host galaxies, implies very high SFRs of ~2500 - 4500 $M_{\odot}yr^{-1}$ in the quasar host galaxies. Even when assuming a significant contribution to the 850μm flux from the quasar itself, very high star formation rates of ~600 - 1500 $M_{\odot}yr^{-1}$ are nevertheless inferred for two of the three detected quasars. We stack the remaining 16 undetected quasars to obtain a 3σ upper limit on the SFR of <880 $M_{\odot}$ yr^{-1} for these quasars.

(ii) Several serendipitous sub-mm detections are found in the 1.5 arcmin radius 850μm maps around each quasar. Considering the 19 fields as a whole, the number counts of these serendipitous detections in the full survey area are consistent with those from blank-field observations. However, several of the individual quasars show evidence for residing in over-dense regions, a conclusion supported by

higher spatial-resolution ALMA observations of several of the quasars.

(iii) We compare the 850μm detection rate of our heavily reddened quasars to both UV-luminous unobscured quasars and the much more highly obscured population of mid-infrared luminous radio-detected HotDOGs. Given the relatively bright flux limits of the 850μm surveys that have been conducted for these populations, the number of detected quasars in each sample is small and there is overall no significant evidence for a difference in 850μm properties.

(iv) The mid-infrared luminous HotDOGs, particularly those selected to host compact radio sources, do however appear to reside in more over-dense regions of the universe compared to our heavily reddened quasars. However, as many of the HotDOGs lack spectroscopic redshifts, further observations are required to confirm the apparent difference.

Given the relatively low detection rate of these heavily reddened quasars with SCUBA-2, a more sensitive dust-continuum survey, e.g. with ALMA, is required to better understand the cool-dust emission properties of the population. ALMA observations would further allow us to obtain spectroscopic identifications for the sub-mm bright sources found around the quasars in the SCUBA-2 maps, and therefore to determine unambiguously whether they are part of the same over-density as the quasar.

ACKNOWLEDGEMENTS

We thank the anonymous referee for a constructive review of the paper. CFW acknowledges funding via an STFC studentship. MB acknowledges funding from The Royal Society via a University Research Fellowship. PCH acknowledges funding from STFC via the Institute of Astronomy, Cambridge, Consolidated Grant. We thank Myrto Symeonidis for providing the quasar template from Symeonidis et al. (2016). Based on observations conducted on the James Clerk Maxwell Telescope as part of Program M17AP008 (PI:Banerji). The James Clerk Maxwell Telescope is operated by the East Asian Observatory on behalf of The National Astronomical Observatory of Japan; Academia Sinica Institute of Astronomy and Astrophysics; the Korea Astronomy and Space Science Institute; Center for Astronomical Mega-Science (as well as the National Key R&D Program of China with No. 2017YFA0402700). Additional funding support is provided by the Science and Technology Facilities Council of the United Kingdom and participating universities in the United Kingdom and Canada. Additional funds for the construction of SCUBA-2 were provided by the Canada Foundation for Innovation.

REFERENCES

Aird J., Coil A. L., Georgakakis A., Nandra K., Barro G., Pérez-González P. G., 2015, Monthly Notices of the Royal Astronomical Society, 451, 1892

Banerji M., McMahon R. G., Hewett P. C., Alaghband-Zadeh S., Gonzalez-Solares E., Venemans B. P., Hawthorn M. J., 2012, Monthly Notices of the Royal Astronomical Society, 427, 2275

Banerji M., McMahon R. G., Hewett P. C., Gonzalez-Solares E., Koposov S. E., 2013, Monthly Notices of the Royal Astronomical Society: Letters, 429, L55

Banerji M., Fabian A., McMahon R., 2014, Monthly Notices of the Royal Astronomical Society: Letters, 439, L51

Banerji M., Alaghband-Zadeh S., Hewett P. C., McMahon R. G., 2015a, Monthly Notices of the Royal Astronomical Society, 447, 3368

Banerji M., et al., 2015b, Monthly Notices of the Royal Astronomical Society, 454, 419

Banerji M., Carilli C., Jones G., Wagg J., McMahon R., Hewett P., Alaghband-Zadeh S., Feruglio C., 2017, Monthly Notices of the Royal Astronomical Society, 465, 4390

Banerji M., Jones G. C., Wagg J., Carilli C. L., Bisbas T. G., Hewett P. C., 2018, Monthly Notices of the Royal Astronomical Society

Barnes J. E., Hernquist L., 1992, Annual review of astronomy and astrophysics, 30, 705

Beelen A., Cox P., Benford D. J., Dowell C. D., Kovács A., Bertoldi F., Omont A., Carilli C. L., 2006, The Astrophysical Journal, 642, 694

Casey C. M., 2012, Monthly Notices of the Royal Astronomical Society, 425, 3094

Casey C. M., et al., 2013, Monthly Notices of the Royal Astronomical Society, 436, 1919

Chapin E. L., Berry D. S., Gibb A. G., Jenness T., Scott D., Tilanus R. P., Economou F., Holland W. S., 2013, Monthly Notices of the Royal Astronomical Society, 430, 2545

Chen C.-T. J., et al., 2013, The Astrophysical Journal, 773, 3

Di Matteo T., Springel V., Hernquist L., 2005, Nature, 433, 604

Edge A., Sutherland W., Kuijken K., Driver S., McMahon R., Eales S., Emerson J. P., 2013, The Messenger, 154, 32

Eisenhardt P. R., et al., 2012, The Astrophysical Journal, 755, 173

Geach J., et al., 2017, Monthly Notices of the Royal Astronomical Society, 465, 1789

Gültekin K., et al., 2009, The Astrophysical Journal, 698, 198

Harrison C. M., et al., 2012, ApJ, 760, L15

Holland W., et al., 2013, Monthly Notices of the Royal Astronomical Society, 430, 2513

Hopkins P. F., Hernquist L., Cox T. J., Di Matteo T., Robertson B., Springel V., 2006, The Astrophysical Journal Supplement Series, 163, 1

Isaak K. G., Priddey R. S., McMahon R. G., Omont A., Peroux C., Sharp R. G., Withington S., 2002, MNRAS, 329, 149

Jones S. F., et al., 2014, Monthly Notices of the Royal Astronomical Society, 443, 146

Jones S. F., et al., 2015, Monthly Notices of the Royal Astronomical Society, 448, 3325

Kennicutt Jr R. C., Evans N. J., 2012, Annual Review of Astronomy and Astrophysics, 50, 531

Kormendy J., Ho L. C., 2013, Annual Review of Astronomy and Astrophysics, 51, 511

Lawrence A., et al., 2007, Monthly Notices of the Royal Astronomical Society, 379, 1599

Lyu J., Rieke G. H., 2017, The Astrophysical Journal, 841, 76

Lyu J., Rieke G. H., Shi Y., 2017, The Astrophysical Journal, 835, 257

Madau P., Dickinson M., 2014, Annual Review of Astronomy and Astrophysics, 52, 415

Magorrian J., et al., 1998, The Astronomical Journal, 115, 2285

McMahon R. G., Banerji M., Gonzalez E., Koposov S. E., Bejar V. J., Lodieu N., Rebolo R., VHS Collaboration 2013, The Messenger, 154, 35

Mor R., Netzer H., 2012, Monthly Notices of the Royal Astronomical Society, 420, 526

Mullaney J., et al., 2012, Monthly Notices of the Royal Astronomical Society, 419, 95

Priddey R. S., McMahon R. G., 2001, Monthly Notices of the Royal Astronomical Society, 324, L17

Priddey R. S., Isaak K. G., McMahon R. G., Omont A., 2003,

Monthly Notices of the Royal Astronomical Society, 339, 1183
Rosario D., et al., 2013, Astronomy & Astrophysics, 560, A72
Rowan-Robinson M., et al., 2018, A&A, 619, A169
Sanders D., Soifer B., Elias J., Madore B., Matthews K., Neugebauer G., Scoville N., 1988, The Astrophysical Journal, 325, 74
Stacey H. R., et al., 2018, MNRAS, 476, 5075
Stanley F., et al., 2017, Monthly Notices of the Royal Astronomical Society, 472, 2221
Symeonidis M., 2017, MNRAS, 465, 1401
Symeonidis M., Giblin B., Page M., Pearson C., Bendo G., Seymour N., Oliver S., 2016, Monthly Notices of the Royal Astronomical Society, 459, 257
Takata T., Sekiguchi K., Smail I., Chapman S. C., Geach J. E., Swinbank A. M., Blain A., Ivison R. J., 2006, ApJ, 651, 713
Temple M. J., Banerji M., Hewett P. C., Coatman L., Maddox N., Peroux C., 2019, MNRAS, 487, 2594
Veilleux S., Kim D.-C., Sanders D., 2002, The Astrophysical Journal Supplement Series, 143, 315
Vestergaard M., Peterson B. M., 2006, The Astrophysical Journal, 641, 689
Wethers C., et al., 2018, Monthly Notices of the Royal Astronomical Society, 475, 3682

This paper has been typeset from a TEX/LATEX file prepared by the author.